

Yield stress effects on fluid displacement in an eccentric annulus

Steinar Kragset and Hans Joakim Skadsem

Norwegian Research Centre AS, Stavanger, Norway

ABSTRACT

As part of well construction operations, steel pipes, called casings or liners, are anchored to the surrounding rock formation by a layer of cement which is placed there in an operation known as primary cementing. Successful cementing is dependent of complete displacement of drilling fluid in the annular space by the cement slurry with minimum intermixing of the fluids. In this paper we study three-dimensional annular fluid displacements using an open source computational fluid dynamics platform. We focus particularly on the effects of fluid yield stresses on iso-density displacements in an eccentric annulus with diameter equal to that of relevant well dimensions.

INTRODUCTION

Construction of wells for geothermal energy recovery or hydrocarbon production proceeds in stages, where the a section of the well is drilled to a target depth and then secured by cementing a casing string or liner to the newly drilled formation. The casing string or liner is cemented to the formation in the operation often referred to as primary cementing where a cement slurry is pumped down the well inside the casing or liner to be cemented. At the bottom, the cement slurry flows out of the casing or liner and back up toward the surface in the annular space between the string and the formation. Once the required volume of cement slurry is injected into the annulus, the slurry is allowed to harden into a solid sheath.

Before cementing, the annulus outside the casing is occupied by the drilling fluid used to drill the current section. An important goal of primary cementing is to completely displace this initial fluid from the annulus and replace it

by cement. It is well established that complete fluid displacement and minimum intermixing of fluids into the cement slurry are important steps for ensuring zonal isolation and a competent annulus cement barrier. Drilling fluids are however normally yield stress fluids that are designed to lift cuttings during drilling and to suspend solids during periods of no circulation. Displacement of such fluids from narrow annuli where the casing string or liner is generally off-centered from the axis of the hole (eccentric) is a delicate operation requiring careful design of fluid densities, viscosities and flow rates.¹¹

Wellbore displacement mechanics are strongly influenced by the annular geometry and governed by the balances between inertia, buoyancy, viscosity as well as fluid properties such as yield stress. Eccentricity results in uneven flow velocities around the casing and potentially static yield stress fluid in the narrow sector.^{5,6}

Under laminar conditions it is generally beneficial to have the displacing fluid as denser and effectively more viscous compared to the displaced fluid. Ideally, a carefully designed fluid hierarchy would result in stable displacements, *i.e.* displacements where the interface between successive fluids translates axially at the imposed bulk velocity. Couturier *et al.*⁴ and later Théron *et al.*⁹ formulated a set of design rules promoting stable displacements in predominantly vertical annuli where an unstable interface is assumed to propagate fastest in the wide sector of the annulus.

It is not always possible to have a large, stabilizing density difference between consecutive fluids due to the resulting hydrostatic head of the column. Excessive wellbore pressure can result in formation fracturing, fluid losses and

unsuccessful cementing. In this paper, we report results from three-dimensional numerical simulations of iso-density displacement flows and focus on the effects of fluid yield stresses in an eccentric annulus with diameter equal to that of relevant well dimensions. We study effects of yield stress in the displaced and in the displacing fluid by varying the Bingham number while maintaining the other dimensionless numbers constant.

PROBLEM FORMULATION

We consider laminar, incompressible and isothermal flows so that the equations governing the annular fluid flow are those of continuity,

$$\vec{\nabla} \cdot \vec{u} = 0, \quad (1)$$

and momentum conservation,

$$\frac{\partial \rho \vec{u}}{\partial t} + \vec{\nabla} \cdot (\rho \vec{u} \vec{u}) = -\vec{\nabla} p + \vec{\nabla} \cdot \boldsymbol{\tau} + \rho \vec{f}. \quad (2)$$

Here, ρ denotes fluid density, \vec{u} is the fluid velocity vector, p is the pressure, $\boldsymbol{\tau}$ is the deviatoric stress tensor and \vec{f} denotes body forces acting on the fluids. Gravity is the only body force included in our simulations.

We focus on an annulus geometry corresponding to a 9 5/8" diameter casing in a 12 1/4" diameter wellbore. This is a common diameter combination for the so-called production casing which is used to isolate producing formations in wells. A competent and isolating annulus cement is critical outside the production casing, making this a relevant annulus geometry for this study.

We next define the degree of casing centralization in the hole, or casing eccentricity defined as $e = \delta / (R_o - R_i)$, where δ is the radial offset between the center of the casing and the center of the hole. If the production casing is run in hole with no centralizers attached, it is fair to assume that the casing collars will contact the borehole wall. A typical 9 5/8" casing will have collars of outer diameter 269.9 mm. This corresponds to an eccentricity of approximately 0.62 away from the collars. Recognizing the importance of good centralization

for successful fluid displacement and cementing, we assume the casing eccentricity is 0.4.

We proceed to non-dimensionalise the governing equations by introducing characteristic length, time and viscosity scales, as per Skadsem *et al.*¹² Denote the radius of the inner cylinder by R_i and the radius of the outer cylinder by R_o . We choose the concentric annulus gap width $d^* = 2(R_o - R_i)$ as characteristic length scale for the displacement flow. The mean or bulk velocity U^* is taken as characteristic velocity scale and $\dot{\gamma}^* = 4U^*/d^*$ is characteristic shear rate. For fluid i , the characteristic effective viscosity is then $\mu_i^* = \mu_i(\dot{\gamma}^*)$. We identify the dimensionless numbers listed in Table 1 for these iso-density displacements.

Table 1. Dimensionless numbers for scaling analysis.

Number	Definition	Description
Re_i	$\frac{\rho_i U^* d^*}{\mu_i^*}$	Reynolds number in fluid i
Bn_i	$\frac{\tau_{y,i} d^*}{\mu_i^* U^*}$	Bingham number in fluid i
n_i		Shear thinning index for fluid i

The Reynolds numbers express the ratio of inertia to viscous stress in the fluids while the Bingham numbers express the ratio of yield stress to viscous stress. In the following section we will define fluid combinations where the Reynolds numbers and shear thinning indices are fixed but where the Bingham number varies.

We consider displacements involving one shear thinning yield stress fluid, fluid 1, and one shear thinning fluid with no yield stress, fluid 2. As the base case, we consider the following Herschel–Bulkley fluid $\tau_1^{(0)} = (5.0 + 0.55 \cdot \dot{\gamma}^{0.75})$ Pa as fluid 1 and the following power law fluid as fluid 2: $\tau_2^{(0)} = \tau_2 = 0.58 \cdot \dot{\gamma}^{0.8}$ Pa. We assume a constant axial flow rate of 1200 l/min which results in $Bn_1 = 1.43$ for the base case. In order to investigate the effect of yield stress on this annulus displacement, we consider two modifications of the fluid 1 parametrization,

namely $\tau_1^{(1)} = (2.5 + 0.70\dot{\gamma}^{0.75})$ Pa and $\tau_1^{(2)} = (10.0 + 0.24\dot{\gamma}^{0.75})$ Pa. These parameter values are chosen so that the effective viscosity of fluid 1 is the same as for the base case at 1200 l/min. This results in the same Reynolds number, but a factor 2 decrease or increase in Bingham number compared to the base case.

The effect of different fluid 1 viscosities can be glanced from the friction pressure gradient as function of flow rate in a concentric annulus geometry of the same diameters as in our problem, shown in Fig. 1. At 1200 l/min, the base

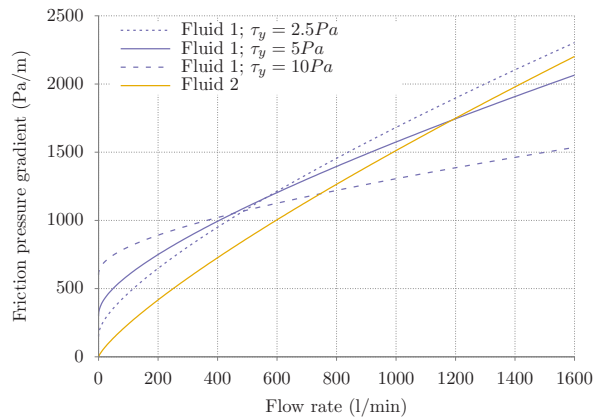


Figure 1. Laminar concentric annulus friction pressure gradients for fluid 1 (base case and two variations) and for fluid 2 (base case).

case results in the same friction pressure gradient in both fluid 1 and fluid 2. For $\tau_1^{(1)}$ with yield stress of 2.5 Pa, the higher consistency index results in a net higher friction pressure gradient at high flow rates. For $\tau_1^{(2)}$, the high yield stress results in a relatively high friction pressure gradient at low flow rates. The friction pressure gradient is however lower than fluid 2 at 1200 l/min.

We investigate separately in the following the cases where fluid 1 is displaced or displacing fluid 2. In each case we investigate the effect of yield stress by varying the fluid 1 viscosity from the base case $\tau_1^{(0)}$ to the modified $\tau_1^{(1)}$ and $\tau_1^{(2)}$.

NUMERICAL METHOD

We solve the governing equations via the interFoam solver from the open-source software OpenFOAM version 5.0,¹ which enables finite-volume computations of multiphase flow with non-Newtonian fluids. In this solver, the volume-of-fluid approach is used, where the fluids are immiscible in the sense that the volume fraction is calculated while the interface is captured. Averages of quantities such as the velocity and density are weighted by the volume fraction of the phases and then used in the continuity and momentum conservation equations. The assumption of immiscibility is considered to be appropriate due to the large difference between the time scale of diffusion and the time scale of the simulations. At the inlet boundary, we prescribe a uniform, axial velocity over the annulus cross-section that is equal to the bulk velocity. No slip conditions are imposed at the walls, however, a short inlet extension is added with free slip conditions to ease the entrance development of the flow. A fixed reference pressure is applied at the outlet. We apply zero gradient boundary conditions for the velocity vector at the outlet and the pressure at the inlet. For more information about the method, the reader is referred to Skadsem *et al.*¹²

A problem when simulating yield stress fluids numerically, is the divergence of the effective viscosity in regions of the flow where the shear rate approaches zero. For practical numerical computations, yield stress fluids are usually regularized, so that the effective viscosity is large but finite in regions where the shear rate is zero. Following initial tests comparing results from an implementation of the Papanastasiou regularization^{3,10} with OpenFOAM's built-in bi-viscosity regularization, we found that the latter gives satisfactory results for the present cases.

The effect of mesh resolution on the axial velocity profile was studied for single-phase flow of the fluid with the highest yield stress, i.e. with Herschel–Bulkley parametrization $\tau_1^{(2)} = (10.0 + 0.24\dot{\gamma}^{0.75})$ Pa, as we assume this to be the most challenging fluid in the

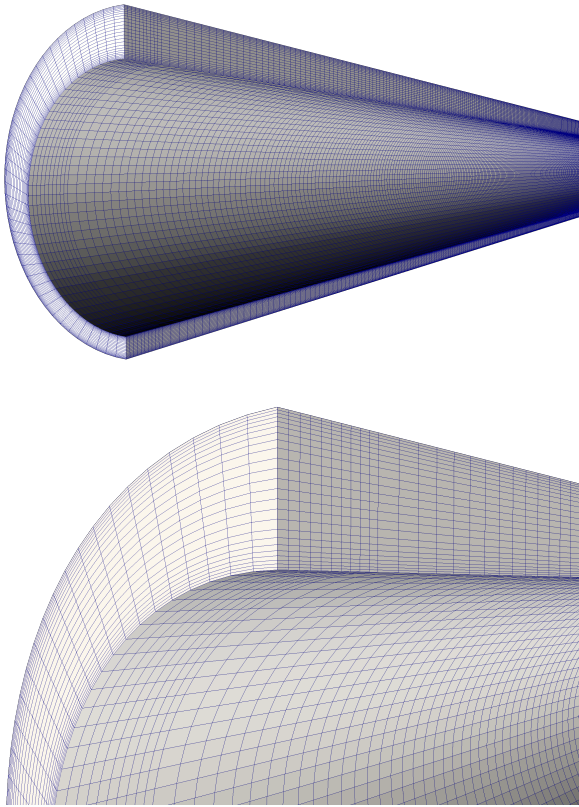


Figure 2. Numerical mesh where half of the system is clipped away to show the internal cell structure. A close-up view is shown below. Note the short entrance section with different mesh resolution, in which free slip conditions are used at the inner and outer walls.

study. We fixed the number of cells in the azimuthal direction to 80, since for symmetry reasons in a concentric annulus this number is not likely to affect the results. We then changed the axial and the radial resolutions independently as shown in Fig. 3, and it was found that the axial resolution hardly affected the results. When compared to the semi-analytical result for the fully-developed, laminar axial velocity profile for the concentric annulus,² we find that the radial resolution significantly affects the accuracy of the numerical results. The peak velocity differs by less than 2 % for all the shown radial resolutions compared to the semi-analytical calculations, but the shoulders of the velocity profile is clearly improved with increased number of cells across the gap.

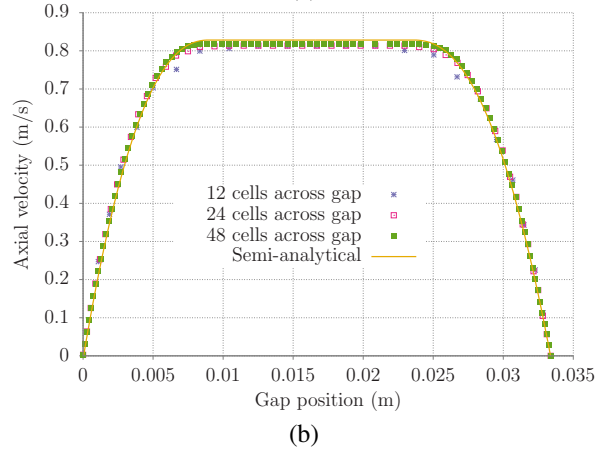
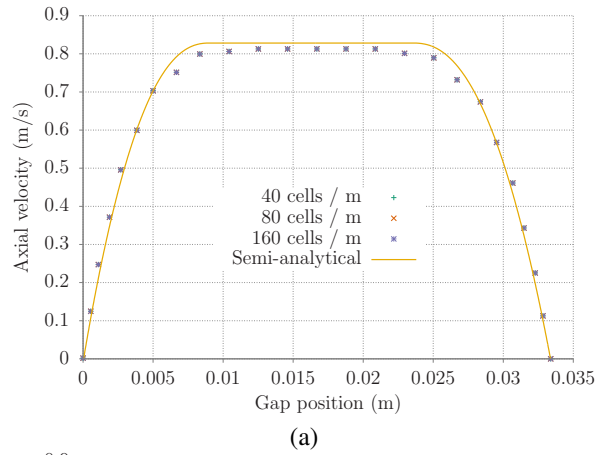


Figure 3. Fully developed axial velocity profile in a concentric annulus for the fluid with the highest yield stress. In the upper plot (a) a fixed number of 12 cells are used across the gap, while the axial density of cells are varied as indicated. In (b) the axial density is fixed at 160 cells/m while the radial number is increased.

In a displacement process in an eccentric annulus there can be significant flow in the azimuthal direction in the vicinity of the interface between the displacing and displaced fluids due to the rearrangement of the axial velocity. Consequently, the importance of azimuthal and axial resolution is increased compared to the single-phase flow in a concentric annulus that was investigated above. To complement the mesh sensitivity study, we monitored the volume concentration, sometimes referred to as the displacement efficiency,^{7,8} during the case PL-HB10 (see Table 2 below for specification

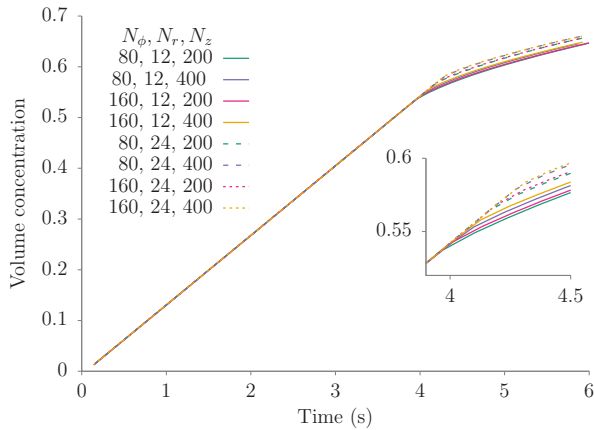


Figure 4. Volume concentration as a function of time in a 5 m long section with eccentricity $e = 0.4$ for various meshes, as indicated. The fluids are specified by case PL-HB10.

of the involved fluids). This is shown in Fig. 4 for various mesh combinations, where N_ϕ , N_r and N_z refer to azimuthal, radial and axial resolutions, respectively. A shortened test section length of 5 m was used.

Only minor differences can be seen in the vol-
Table 2. Simulated displacement cases and parametrizations.

Case name	Displacing fluid			Displaced fluid		
	τ_y (Pa)	K (Pa s ^{<i>n</i>})	n (-)	τ_y (Pa)	K (Pa s ^{<i>n</i>})	n (-)
PL-PL	-	0.58	0.8	-	0.58	0.8
PL-HB2	-	0.58	0.8	2.5	0.70	0.75
PL-HB5	-	0.58	0.8	5.0	0.55	0.75
PL-HB10	-	0.58	0.8	10	0.24	0.75
HB2-PL	2.5	0.70	0.75	-	0.58	0.8
HB5-PL	5.0	0.55	0.75	-	0.58	0.8
HB10-PL	10	0.24	0.75	-	0.58	0.8

ume concentration, however, the largest influence is still produced by variations in the radial resolution. We conclude that satisfactory accuracy can be achieved for the current study with $N_\phi = 80$ and $N_r = 24$ and with 80 cells per meter in the axial direction, i.e. $N_z = 400$ when the length is 5 m.

For the remainder of this work, the axial length is 10 m, not including the aforementioned inlet extension, which is 0.05 m. The cases are summarized in Table 2.

RESULTS

In all the cases, the fluid to be displaced is initially at rest and filling the entire domain, and at the start of the simulation the inlet velocity is linearly ramped up from zero to a uniform and steady 0.686 m/s after 0.1 s simulated time in order to smooth the development of the flow. This is a small time scale compared to the time scale of interest and can safely be ignored when analysing the results.

The volume concentration of the displacing fluid in the volume starting immediately after the inlet extension and stretching axially for 8 m is shown for all the cases in Fig. 5. The last 2 m of the simulation cases are not included in order to avoid any outlet effects. The overall trend for the curves is typical with a linear section indicating that the displaced fluid is in the beginning flowing out of the monitored region with the bulk flow rate. After some time, the rate decreases due to the non-uniform profile of the displacement front. The ideal case would be a piston-like displacement where the linear part extended all the way to a volume concentration of 1, meaning that all of the initial fluid is removed and 100 % displacement efficiency is achieved in the shortest possible time for the given flow rate. It can be seen that increasing yield stress in the displaced fluid decreases the efficiency, however the effect is small for our cases. The deviation from linear behaviour of the efficiency, i.e. the volume concentration of the displacing fluid, can mainly be attributed to the non-uniform velocity profile due to the eccentricity of the annular region.

In Fig. 6 a three-dimensional representation of the displacement process is shown for the PL-PL case. In this case the displaced and displacing fluids are identical power law fluids, which means that the displacement process is given purely by the development of the single-phase velocity profile. In contrast, displacement by the power law fluid of the Herschel–Bulkley fluid with the highest yield stress is shown in Fig. 7. Here, the propagation of the displacement front is slower, but at the same time the front is not stretched as much due to the azimuthal flows that rearrange the velocity

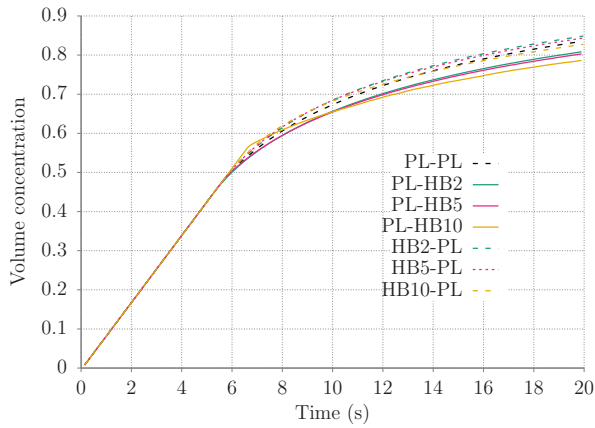


Figure 5. Volume concentration of the displacing fluid. Dashed lines are for displacements of the power law fluid.

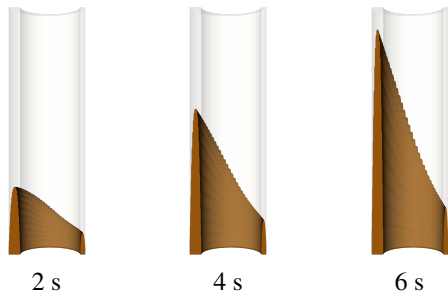


Figure 6. Case PL-PL. Regions where the volume concentration of displacing fluid is higher than 0.2 at indicated times.

profile from that of the Herschel–Bulkley fluid to the power law fluid’s profile.

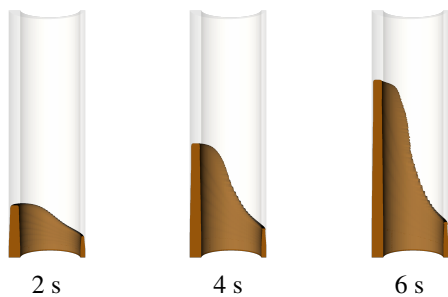


Figure 7. Case PL-HB10. Regions where the volume concentration of displacing fluid is higher than 0.2 at indicated times.

A different representation of the two cases is given in Figs 8 and 9, where the volume concentration of the displacing fluid is averaged across the gap and plotted in the azimuthal–

axial space.

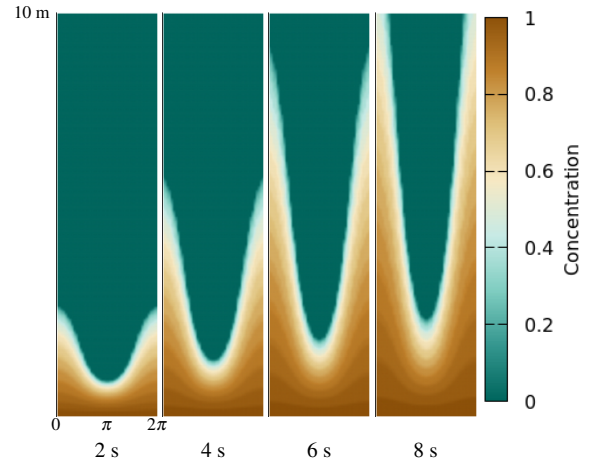


Figure 8. Gap averaged volume concentration of displacing fluid for the PL-PL case. Times, azimuthal and axial coordinates are indicated.

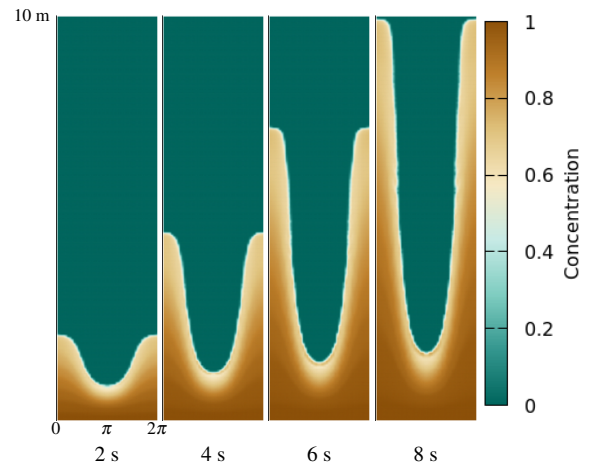


Figure 9. Gap averaged volume concentration of displacing fluid for the PL-HB10 case. Times, azimuthal and axial coordinates are indicated.

One of the benefits with three-dimensional simulations is the opportunity to study the radial structure of the displacement front. In Fig. 10 contours for a 0.2 volume concentration of displacing fluid is shown at 6 s after the start for the cases with increasing yield stress in the displaced fluid. The contours are shown across the widest and narrowest parts of the annulus. The front gets more flat and piston-like, both in the wide and narrow gaps, when the yield stress

increases. However, a wall layer of undisplaced fluid seems to extend far behind the front in all the cases, as do the displacement front on the narrow side compared to the wide side. When the Herschel–Bulkley fluids are used as the displacing and the power law fluid is the fluid to be displaced, we find only minor effects of increased yield stress, as shown in Fig. 11.

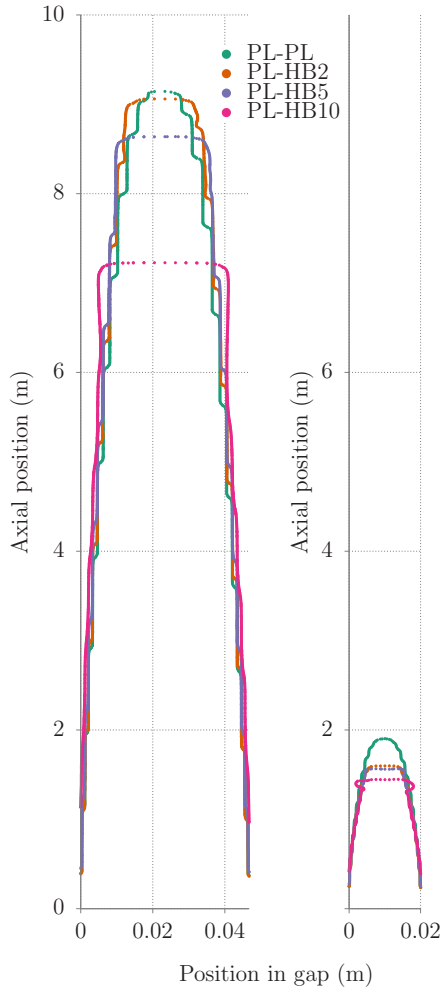


Figure 10. Contours for 0.2 volume concentration of displacing fluid across the wide (left) and narrow (right) gaps at 6 s, comparing displaced fluids with increasing yield stress.

SUMMARY AND CONCLUSIONS

Density and viscosity stable fluid combinations are considered beneficial for laminar displacement flows during cementing of casings

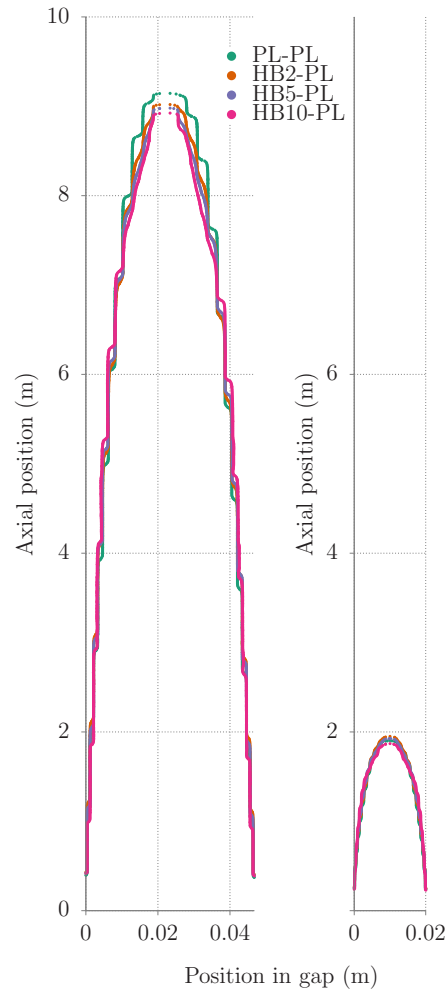


Figure 11. Contours for 0.2 volume concentration of displacing fluid across the wide (left) and narrow (right) gaps at 6 s, comparing displacing fluids with increasing yield stress.

and liners. Due to constraints such as formation fracturing pressure, it is not always possible to achieve a significant, stabilizing density difference between the fluids. In this paper we have investigated the role of viscosity and yield stress in particular on iso-density laminar displacement efficiency in a near-vertical, eccentric annulus using numerical simulations. The fluid viscosities have been adjusted so that the effective viscosity is unchanged as the yield stress is varied; this results in constant Reynolds numbers but varying Bingham numbers between fluid combinations.

In the absence of density differences, the difference in axial velocity profiles between the two fluids results in azimuthal and radial flow close to the interface between the fluids. We observe fairly small effects of changing the Bingham number in these simulations; the most significant effect of yield stress is observed when the displaced fluid is a yield stress fluid, Fig. 10. Increasing the yield stress of the displaced fluid results in a flatter interface between the fluids. The effects of yield is less pronounced when the displaced fluid is a power law fluid and the displacing fluid exhibits varying magnitudes of yield stress, Fig. 11. In all cases, the interface front in the narrow sector lags far behind the front in the wide sector, and wall layers extend far beyond the front of the interface. For the parameter range considered in this paper, increasing the density contrast between the consecutive fluids (if possible) is likely to be more effective in diverting flow azimuthally between wide and narrow sectors in an eccentric annulus.¹³

ACKNOWLEDGEMENTS

The Research Council of Norway, ConocoPhillips, AkerBP, Equinor and Winterhall are acknowledged for financing the work through PETROMAKS project number 244577/E30 and the research centre DrillWell - Drilling and Well Centre for Improved Recovery, a research cooperation between NORCE, NTNU, SINTEF and UiS.

REFERENCES

1. OpenFOAM, <http://www.openfoam.org>.
2. Hanks, R. W. (1979), "The Axial Laminar Flow of Yield-Pseudoplastic Fluids in a Concentric Annulus", *Ind. Eng. Chem. Process Des. Dev.*, **18**, 488 - 493.
3. Papanastasiou, T. C. (1987), "Flows of Materials with Yield", *Journal of Rheology*, **31**, 385-404.
4. Couturier, M., Guillot, D., Hendriks, H. and Callet, F. (1990), "Design Rules And Associated Spacer Properties For Optimal Mud Removal In Eccentric Annuli", in "CIM/SPE International Technical Meeting",.
5. Walton, I. C. and Bittleston, S. H. (1991), "The axial flow of a Bingham plastic in a narrow eccentric annulus", *J. Fluid Mech.*, **222**, 39 - 60.
6. Szabo, P. and Hassager, O. (1992), "Flow of viscoplastic fluids in eccentric annular geometries", *J. Non-Newtonian Fluid Mech.*, **45**, 149 - 169.
7. Tehrani, A., Ferguson, J. and Bittleston, S. H. (1992), "Laminar Displacement in Annuli: A Combined Experimental and Theoretical Study", in "SPE Annual Technical Conference and Exhibition, 4-7 October",.
8. Tehrani, M. A., Bittleston, S. H. and Long, P. J. G. (1993), "Flow instabilities during annular displacement of one non-Newtonian fluid by another", *Experiments in Fluids*, **14**, 246 - 256.
9. Théron, B. E., Bodin, D. and Fleming, J. (2002), "Optimization of Spacer Rheology Using Neural Network Technology", in "IADC/SPE Drilling Conference",.
10. Frigaard, I. A. and Nouar, C. (2005), "On the usage of viscosity regularisation methods for visco-plastic fluid flow computation", *J. Non-Newtonian Fluid Mech.*, **127**, 1-26.
11. Nelson, E. B. and Guillot, D. (2006), "Well Cementing", Schlumberger.
12. Skadsem, H. J., Kragset, S., Lund, B., Ytrehus, J. D. and Taghipour, A. (2019), "Annular displacement in a highly inclined irregular wellbore: Experimental and three-dimensional numerical simulations", *J. Petrol. Sci. Eng.*, **172**, 998-1013.
13. Skadsem, H. J. and Kragset, S. (2019), "Effect of Buoyancy and Inertia on Viscoplastic Fluid: Fluid Displacement in an Inclined Eccentric Annulus With an Irregular Section. Part 2: Displacements in Vertical Annulus", in "ASME 2019 38th International Conference on Ocean, Offshore and Arctic Engineering",.